Chinese Journal of Aeronautics, (2016), 29(2): 386–394

Chinese Society of Aeronautics and Astronautics
& Beihang University

Chinese Journal of Aeronautics

cja@buaa.edu.cn
www.sciencedirect.com

Precessing motion in stratified radial swirl flow

Qin Hao [a], Lin Yuzhen [a,*], Li Jibao [b]

[a] National Key Laboratory of Science and Technology on Aero-Engine Aero-thermodynamics, School of Energy and Power Engineering, Beihang University, Beijing 100083, China
[b] AVIC Commercial Aircraft Engine Co., Ltd., Shanghai 200241, China

Received 23 January 2015; revised 27 July 2015; accepted 30 October 2015
Available online 23 February 2016

KEYWORDS

Large eddy simulation;
Precessing motion;
Stratified flow;
Swirl flow;
Unsteady flow

Abstract Vortex/flame interaction is an important mechanism for unsteady combustion in a swirl combustion system. Technology of low emission stirred swirl (TeLESS), which is characterized with stratified swirl flow, has been developed in Beihang University to reduce NO_X emission. However, large-scale flow structure would be induced in strong swirl flow. Experiments and computational fluid dynamics (CFD) simulation were carried out to investigate the unsteady flow feature and its mechanism in TeLESS combustor. Hotwire was firstly applied to testing the unsteady flow feature and a distinct mode with 2244 Hz oscillation frequency occurred at the pilot swirl outlet. The flow mode amplitude decayed convectively. Large eddy simulation (LES) was then applied to predicting this flow mode and know about its mechanism. The deviation of mode prediction compared with hotwire test was 0.8%. The spiral isobaric structure in pilot flow passage indicates that precessing vortex core (PVC) existed. The velocity spectrum and phase lag analysis suggest that the periodic movement at the pilot outlet was dominated by precessing movement. Negative tangential momentum gradient reflects that the swirl flow was unstable. Another phenomenon was found out that the PVC movement was intermittently rotated along the symmetric axis.

1. Introduction

Green energy is the topic of 21st century. As for aero gas turbine combustor, lean combustion technologies are developed, such as lean premixed prevaporized (LPP), lean direct injection (LDI) and rich burn-quench-lean burn (RQL), to reduce NO_X emission.[1,2] However, lean combustion system is susceptible to the combustion instability, which is a resonant phenomenon coupled between unsteady heat release and acoustic mode of combustor. This instability occurs with large amplitude of periodic pressure or velocity oscillation in combustor, leads to the failure of high-temperature component and finally threatens the engine's safety.[3,4]

Technology of low emission stirred swirl (TeLESS) for civil aero-engine combustor was developed in Beihang University to reduce NO_X emission. Concentric staged partial premixed combustion is applied to this technology, in which the multi-hole-air-injection is adopted in main stage to generate the premixed flame and single fuel spray is adopted to realize the diffusion combustion to stabilize main stage flame.[5] In terms

* Corresponding author. Tel.: +86 10 82316847.
E-mail addresses: hao916200@163.com (H. Qin), linyuzhen@buaa.edu.cn (Y. Lin), li9403@hotmail.com (J. Li).
Peer review under responsibility of Editorial Committee of CJA.

Production and hosting by Elsevier

http://dx.doi.org/10.1016/j.cja.2016.02.004
1000-9361

of partial premixed swirling combustion, two mechanisms dominate the unsteady combustion, the first one is equivalence ratio oscillation, the second one is vortex/flame interaction.[6] Equivalence ratio oscillation time lag phenomenon was observed and proposed by Lieuwen et al.,[7] Lee et al.[8] and Nguyen[9] measured the equivalence ratio oscillation through infrared absorption using 3.39 μm HeNe laser system. Large eddy simulation was applied by Huang and Yang[10] to investigate the interaction between large-scale flow structure and flame in a model swirl combustor. Large eddy simulation was also applied by Sengissen et al.[11] in a stratified swirl combustion system and the interaction between pilot stage spray flame and precessing vortex was confirmed as the nonlinear mechanism. Bellow et al.[12] studied the nonlinear flame transfer function in a swirl stabilized model combustor. The rolling up and shedding movements of flame were the saturation mechanism. Several phenomena were observed in Balachandran et al's study.[13] In turbulent swirl premixed combustion system, small disturbance with higher exciting frequency would be easier to cause the rolling up of flame in shear layer, and the critical disturbance would get larger with increasing equivalence ratio.

As for swirl flow, symmetry ring vortex and asymmetry spiral vortex would be observed in common under large swirl number.[14,15] The unsteady flow mode can be described by Strouhal number (St), and this dimensionless number is almost independent of flow Reynolds number.[14] In aeroengine combustor, the swirl number is generally designed around 0.6 to generate a stale centroid recirculation to stabilize the flame.[16] Under this circumstance, ring vortex or spiral vortex would occur. Questions are raised as to whether the large-scale flow structure would occur in TeLESS combustor and where they would be produced and developed. In order to answer those questions, unsteady flow feature is firstly diagnosed using hotwire measurement and the corresponding mechanism is then studied by large eddy simulation. Syred[14] has described that 1. Processing vortex core(PVC) mode frequency(f_0) is quasi-linear with the bulk flow velocity; 2. The intensity of PVC movement relies on the fuel/air mixing properties in partial premixed combustion; 3. The PVC mode frequency changes from f_0 to (0.8–1)f_0 with non-reacting flow condition transited to partially premixed reacting flow condition. Consequently, the present investigation was carried out under non-reacting flow condition (without combustion), because it is conductive to cost reduction and urgent technology transition on single nozzle test research period.

2. Experiment

Instantaneous flow velocity at the adjacent downstream of TeLESS swirler was measured by 1D-hotwire. As the unsteady flow mode was most concerned in this study, less attention was paid to three-dimensional character of swirl flow and the datas obtained from 1D-hotwire is enough. The test system is illustrated in Fig. 1. The flow rate was controlled by upstream valve and displayed by differential pressure sensor indirectly because the bulk flow velocity U is proportional to the square of pressure drop ΔP when flow Mach number is smaller than 0.2. The hotwire probe was arranged at downstream of swirler and was installed onto the displacement component, which has a displacement resolution of 2.5 μm. Transparent organic glass tube was applied to adjusting the hotwire probe. The hotwire

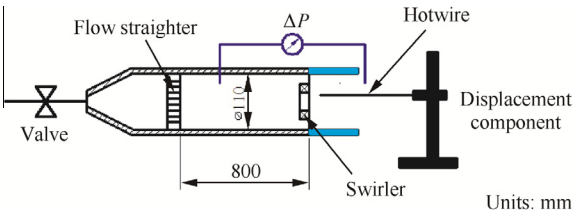

Fig. 1 Hotwire test system.

probe arrangement is illustrated in Fig. 2; the hotwire was parallel to the radial direction of swirler. The tangential velocity w, satisfying the right-hand rule, is defined as positive. The plane $x0y$ is perpendicular to the ground.

Scheme of TeLESS swirler is illustrated in Fig. 3, where three swirlers are concentric and the flow is referred to as stratified flow. The main stage inlet is perforated. And the pilot is combined by two counter radial swirlers. The swirl number of 1st and 2nd swirler at pilot stage is 0.67 and −0.72 respectively, and the swirl number at main stage is −0.6. The negative sign means the counter rotating direction. The variable R_P is the radius of the pilot outlet. The pressure drop cross swirler (ΔP) during the test was to ensure that the bulk velocity under atmosphere condition was equal to takeoff design condition in real engine combustor. ΔP = 3.92 kPa was applied and the corresponding flow Reynolds number of pilot stage outlet and main stage outlet was 1.16×10^5 and 2.97×10^5 respectively.[17] The hydraulic diameter of each stage outlet was applied in estimating the Reynolds number. In order to know the spatial feature of this stratified swirl flow, the flow velocity at different position was scanned. The scanning was carried out in the $x0y$ plane (see Fig. 2) and the scanning grids are illustrated in Fig. 3 as well. The grid

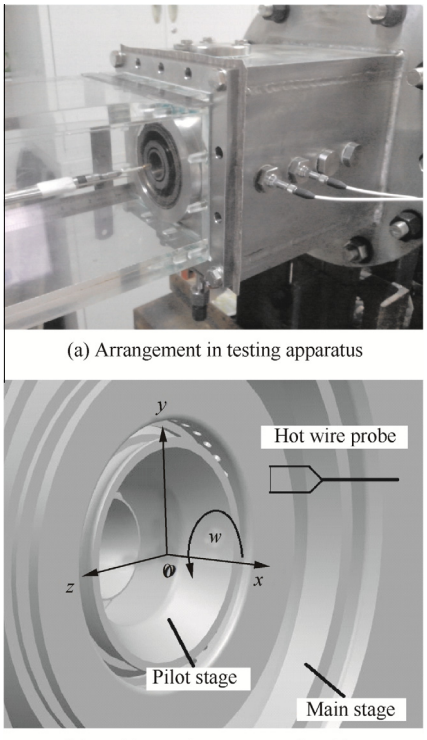

(a) Arrangement in testing apparatus

(b) Position at downstream of swirler

Fig. 2 Hotwire arrangement.

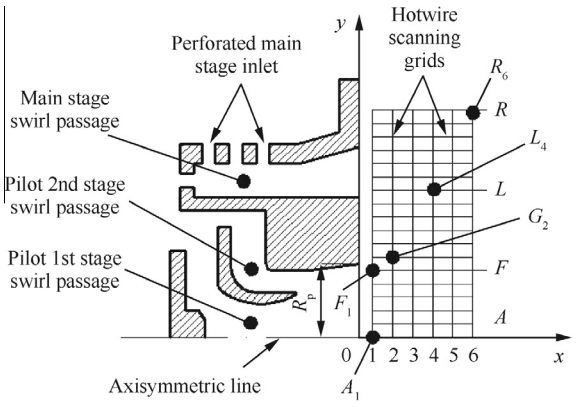

Fig. 3 Scheme of TeLESS swirler and hotwire scanning grids.

nodes position in radial direction was represented by capitals from A to R (some capitals are absent) and the position in axial direction was represented by numerals from 1 to 6. The axial interval was 3 mm, and the radial interval was 2 mm. The position of node A_1 was located 2 mm downstream from the center of the pilot outlet. For instance, the positions of nodes A_1, F_1, G_2, L_4 and R_6 in plane $x0y$ were (2,0), (2,10), (3,12), (9,22) and (15,34), respectively. The origin of Cartesian coordinate is at the center of pilot stage outlet; the position of A_1 is at 2 mm downstream of pilot stage outlet; the physical space between adjacent Arabic notation on abscissa is 3 mm; the physical space between adjacent capital letter on ordinate is 2 mm. The sample rate of hotwire was 20 kHz and 2 seconds' data was recorded at each node.

Statistic and fast fourier transform (FFT) were applied to obtaining the average velocity and the unsteady flow velocity spectrum. Original time domain signal is illustrated in Fig. 4 (a), the ordinate u represents velocity, the mean velocity at F_1 node was 42.77 m/s. FFT was then performed and two periodic flow modes can be recognized in Fig. 4(b), the ordinate u' represents velocity oscillation component. The first mode was 1126 Hz with amplitude of 1.09 m/s and the second mode was 2244 Hz with amplitude of 3.27 m/s. Compared with the first flow mode, the second one was much more distinct. That is, the periodic flow was dominated by the second mode. Band pass filter at 2244 Hz with half-bandwidth of 5 Hz is illustrated in Fig. 4(c). It is found that the second flow mode is in perfect sinusoidal motion. Positions at which second flow mode existed in the test are illustrated in Fig. 5 and are pointed out as black spot. The second mode just occurs in the adjacent region of pilot outlet. The absolute values of velocity fluctuating amplitude of the second mode at each position were different; the oscillation amplitude was the largest near the shear layer boundary and decays convectively. Velocity information at three positions, E_1, F_1, G_2, is listed in Table 1.[17]

3. Large eddy simulation

Large eddy simulation (LES) was applied to analyzing the periodic flow motion mentioned above. As the perforation is adopted for main stage inlet, simplification of calculation domain for main stage passage was carried out to reduce the complexity level. This simplification method was referred to the method once applied in Zhang et al's[18] CFD simulation on NO_X emission of TeLESS combustor. Moreover, the periodic flow motion just occurred locally at pilot stage.[19] Thus it is reasonable to make a simplification for the main stage passage flow domain.

Unstructured mesh was applied for calculation domain. Due to the sensitivity of large eddy simulation to the mesh number and quality, the mesh dimension ΔL is shown as

$$\Delta L = \bar{u}\Delta t \tag{1}$$

in which, Δt is time resolution (time step) and $\bar{u}$ is the local mean velocity. As the second flow mode was 2244 Hz obtained from hot wire test, the period was about 4.5×10^{-4} s. In order to capture the dynamic process, time resolution is set as $\Delta t = 1 \times 10^{-5}$ s, and there are 45 segments to describe a complete periodic movement. In addition, as the local mean velocity at position of F_1 node was 42.77 m/s, the displacement of fluid particle was about 0.43 mm in a single time segment. Thus, the mesh dimension should be satisfied $\Delta L < 0.43$ mm when establishing unstructured mesh. The grid independence was performed using Reynolds-averaged Navier–Stokes (RANS) equations with 2.6 million, 3.2 million and 3.9 million grids. Fig. 6 shows the axial velocity profiles at different axial positions with different grid numbers. It can be seen that the axial velocity profile changes little when the grids number exceeds 3.2 million. Consequently, the mesh with 3.2 million grids was selected for simulation.

As for boundary condition, the outlet of calculation domain is set as pressure outlet boundary. And the pilot stage inlet and main stage inlet are set as mass flow rate inlet boundary after considering the low flow Mach number ($Ma < 0.2$) in

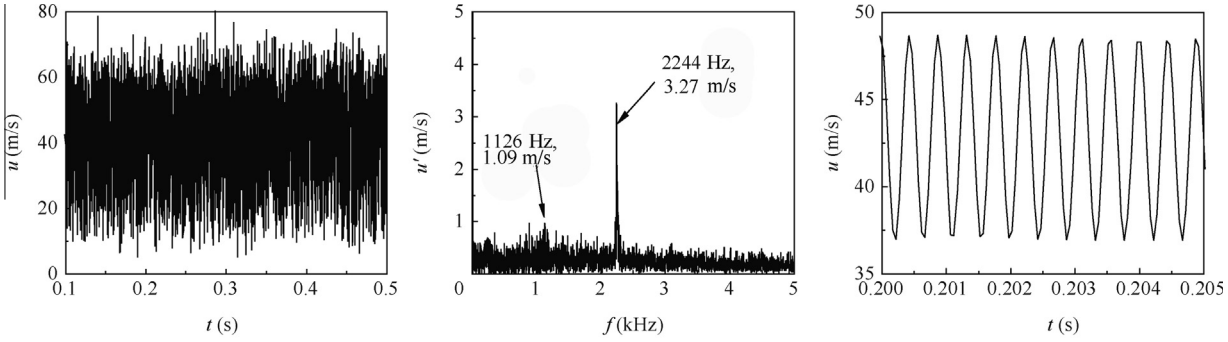

(a) Unsteady flow velocity in time domain

(b) Unsteady flow velocity spectrum in frequency domain

(c) Band-pass filter at 2244±5 Hz of unsteady flow velocity

Fig. 4 Hotwire test results at position of F_1 node.

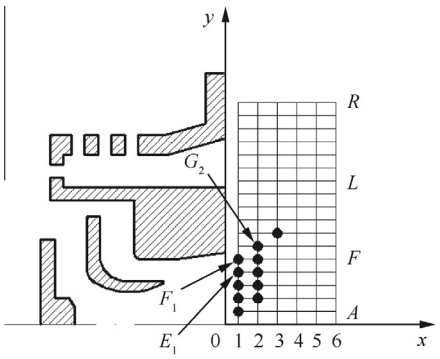

Fig. 5 Region impacted by the second periodic flow mode (hotwire test result).

Table 1 Unsteady flow tested by hotwire.[17]

Node number	Mean velocity $\bar{u}$ (m/s)	Second mode f(Hz)	Mode amplitude A_u (m/s)
E_1	25.88	2256	2.00
F_1	42.77	2244	3.27
G_2	41.21	2232	2.32

swirler and the simplification of calculation domain for upstream of swirler. The mass flow rate m_a is deduced from pneumodynamics, seen as Eqs. (2)–(4).

$$m_a = \frac{K\sqrt{T^*}}{P^*} A_e q(\lambda) \tag{2}$$

$$\lambda = \frac{U}{c_{cr}} = \frac{U}{\sqrt{\frac{2\gamma}{\gamma+1} RT^*}} \tag{3}$$

$$U = \sqrt{\frac{2\Delta P}{\rho}} = \sqrt{\frac{2\Delta P}{\frac{P}{RT}}} \approx \sqrt{\frac{2\Delta P}{\frac{P^*}{RT^*}}} \tag{4}$$

In which,the variable A_e is the effective flow area of swirler, K is a constant, $q(\lambda)$ is aerodynamic function value, c_{cr} is critical sound speed, γ is the ratio of specific heat, R is the gas constant, P^* and T^* represent total pressure and total temperature respectively.

Wall-adapting local eddy viscosity (WALE) subgrid-scale model was applied. In order to reduce the convergence time, initial solution was first obtained by RANS and then imported into LES simulation. In order to validate the LES, flow velocity and its components in three directions at several positions (including E_1, F_1, G_2) were recorded at each time step in LES. The sample time step was 1×10^{-5} s and 0.2 million time steps were recorded.

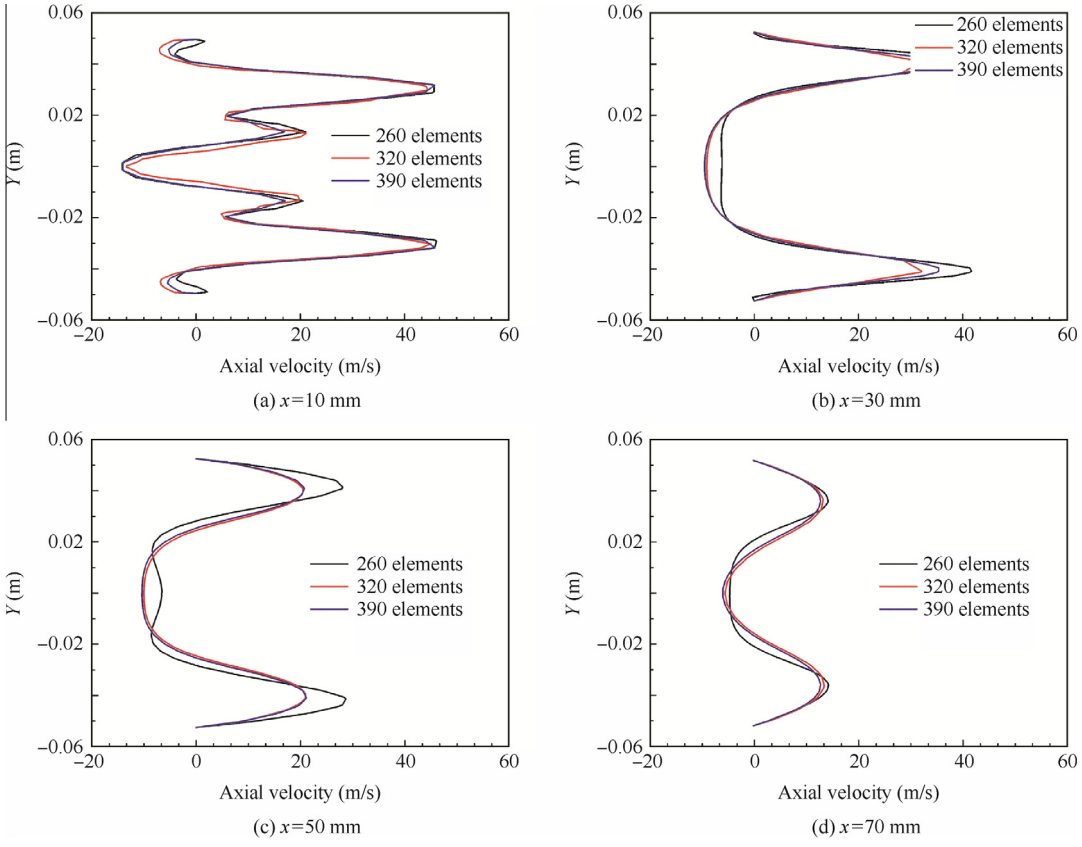

Fig. 6 Grid independence validation using RANS results.

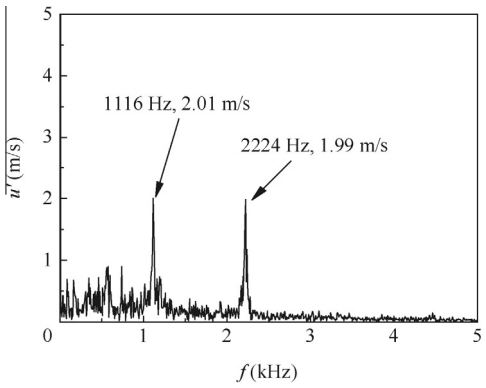

Fig. 7 Unsteady flow velocity spectrum at position of F_1 node obtained from LES.

Table 2 Unsteady flow predicted by LES.

Node Number	Mean velocity $\bar{u}$(m/s)	Second mode f (Hz)	Mode amplitude A_u (m/s)
E_1	25.83	2224	1.11
F_1	44.66	2224	1.99
G_2	28.02	2224	1.29

Velocity spectrum at position of F_1 node obtained from LES is illustrated in Fig. 7. Two flow modes can be distinguished from the spectrum as well. The first mode was 1116 Hz with amplitude of 2.01 m/s and the second mode was 2224 Hz with amplitude of 1.99 m/s. Compared with the hotwire test result, the frequency simulation deviation is about 0.8%. However, the amplitude simulation deviation is quite large. The simulation result of amplitude of the first mode was an order larger than test, and the second mode was near half smaller than test. This large deviation on amplitude would be due to the initial background flow obtained from RANS. This phenomenon could be explained as that the energy switched between 1st mode and 2nd mode. Hirshi et al.[20] once found out that the initial trigger condition has a great influence on the motion in the nonlinear system, which manifests itself in the form of different amplitudes. Unsteady velocity information at positions E_1, F_1, G_2 is listed in Table 2. The second mode frequency simulation deviated from test results less than 1.4%. Although the amplitude simulation deviated greatly away from test result, the spatial distribution of oscillation amplitude was familiar with test. In total, unsteady flow mode in TeLESS swirl can be captured by LES. As the second flow mode dominates in the hotwire test, this mode will be used for analysis in discussion.

4. Discussion

This section discusses the basic features of flow velocity fluctuation, the reason leading to those features and the influence of precessing motion on swirl flow stability.

Phase relationships between flow velocity u and its three direction velocity components u_x, u_y, u_z are illustrated in Fig. 8, which are obtained by band-pass filter at the center frequency of 2224 Hz with bandwidth of 10 Hz. Because the position of F_1 node is located in the $x0y$ plane, the components u_x, u_y, u_z correspond to axial, radial and tangential direction respectively. It was found out that the flow velocity u was in phase with axial component u_x, but out of phase with the radial component u_y and tangential component u_z. The tangential component u_z lagged off axial component u_x about 136°. In addition, the fluctuating amplitude of tangential component was 3 times larger than that of axial component; however, the fluctuation of velocity u was still dominated by axial component. The reason of this phenomenon is that the absolute magnitude of axial component at position of F_1 node was much larger than that of tangential component. As a result, the velocity u was in phase with the former component. This conjecture can be deduced from the correlation $|u| = \sqrt{|u_x|^2 + |u_y|^2 + |u_z|^2}$.

A spiral isobaric surface (99500 Pa) selected at arbitrary time in the pilot passage is illustrated in Fig. 9, and this asymmetric structure is referred as precessing vortex core (PVC).[21,22] Question is raised as to whether the periodic velocity fluctuation at F_1 node is caused by this precessing motion. Velocity spectrums and phase relationships at four special positions (S_1, S_2, S_3, S_4) in pilot passage are analyzed, these four position and the corresponding spectra are illustrated in Fig. 10. Velocities at positions S_1 and S_2 reflect the unsteady flow features in 1st swirl of pilot stage, while the S_4 reflects feature in 2nd swirl. The velocity at position S_3 represents the shear layer's feature.

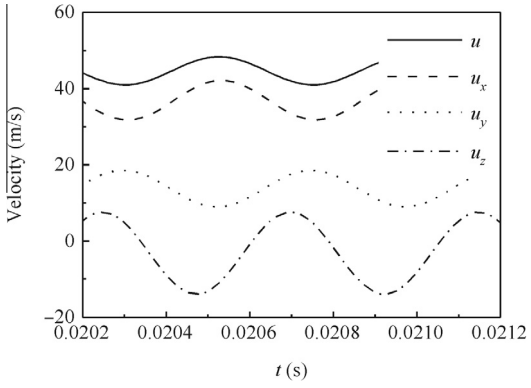

Fig. 8 Phase relationship between flow velocity u and its three direction velocity components u_x, u_y, u_z (LES result).

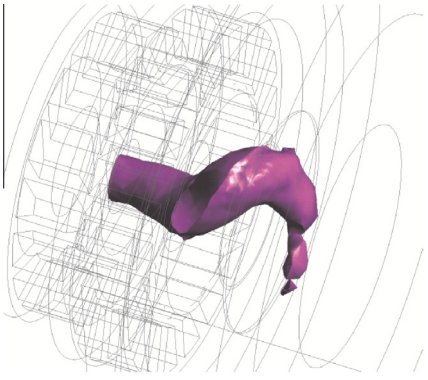

Fig. 9 Isobaric surface (99500 Pa) at arbitrary time (LES result).

Unsteady flow modes of 1120 Hz and 2244 Hz both can be seen in 1st and 2nd swirl passage; however, the amplitude at 1st swirl was almost an order larger than 2nd swirl. This phenomenon indicates that the velocity fluctuation in 2nd swirl was induced by the background pressure fluctuation which was caused by the precessing motion in 1st swirl passage. The phenomenon that the amplitude at S_1 is smaller than S_2 implies that the precessing motion was in initial period at S_1 and reached full development at S_2. The amplitude at S_3 was sharply reduced compared with S_2's, which shows that flow shear between 1st and 2nd swirl had significant damping effect on precessing motion. Finally, the precessing motion intensity decayed convectively as the amplitude at F_1 was smaller than S_3. The phase relationships (Fig. 10(f)) between S_2, S_3 and F_1 depict the axial convective feature.

Swirl flow stability and criteria were studied and proposed by Rayleigh[23]:

(1) The swirl flow is stable when tangential momentum moment ρwr increase along radial direction.
(2) The swirl flow is neutrally when ρwr keeps constant along radial direction.
(3) The swirl flow is unstable when ρwr decrease along radial direction.

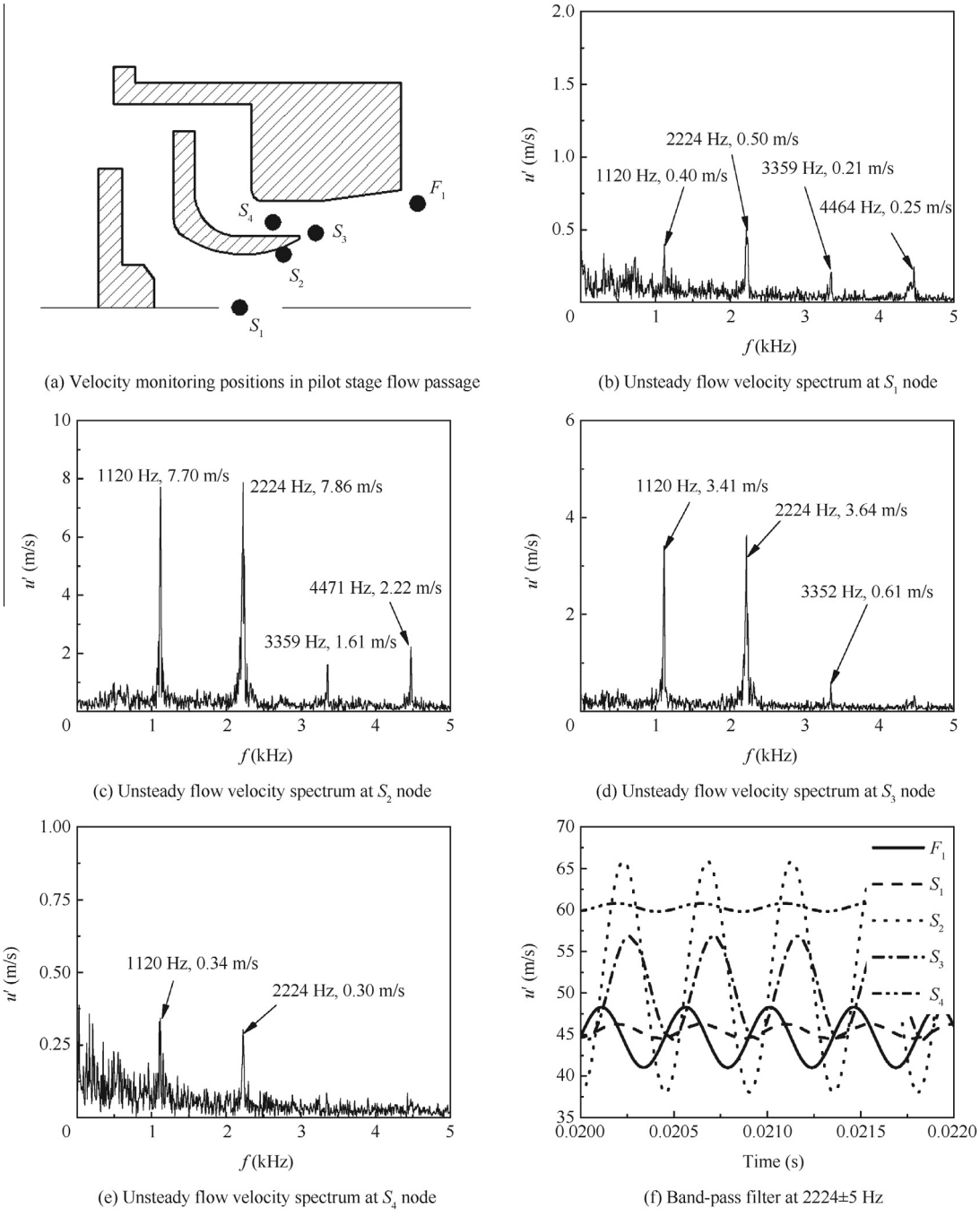

(a) Velocity monitoring positions in pilot stage flow passage

(b) Unsteady flow velocity spectrum at S_1 node

(c) Unsteady flow velocity spectrum at S_2 node

(d) Unsteady flow velocity spectrum at S_3 node

(e) Unsteady flow velocity spectrum at S_4 node

(f) Band-pass filter at 2224±5 Hz

Fig. 10 Unsteady flow features in pilot passage (LES result).

A modified Richardson number (Ri^*) is proposed by Beer et al.[24] to describe the stability of swirl flow system. The system becomes stable if Ri^* is larger than zero. The radial distributions of ρwr at different phases at the position of $x = 2$ mm (passing through F_1 node) are illustrated in Fig. 11. R_p is the radius of pilot outlet (see Fig. 3). It can be found out that there are four flow characteristic regions in pilot swirl flow. In the region of $0 < r/R_p < 0.35$, the gradient $d(\rho wr)/dr$ almost kept zero, which indicates that free vortex existed. In the region of $0.35 < r/R_p < 0.5$, $d(\rho wr)/dr$ kept positive, which indicates that the flow was stable and the flow behaved as solid rotation. However, in the region of $0.5 < r/R_p < 0.9$, $d(\rho wr)/dr$ turned to negative, which indicates that the flow was unstable. This is because that the full development of precessing motion would bring flow system into unstable. Due to the boundary layer flow, the gradient $d(\rho wr)/dr$ turned back to positive. And the negative minimum of ρwr corresponds to the maximum velocity fluctuation amplitude. These two phenomena indicate that there was little effect of precessing motion on boundary layer flow.

The reference[25] has mentioned that the PVC rotates around recirculation zone, sheds and convects along stream line where axial velocity equals zero. That is, once there was PVC in the swirl flow, the position where $u_x = 0$ around recirculation zone represents the PVC position. Velocity ratio u_z/u_x is introduced here to estimate the radial position of PVC. As $u_x \to 0$, u_z/u_x became the largest. The reason why applying component u_z is that this component fluctuated strongest. The radial distributions of velocity ratio at different phase are illustrated in Fig. 12. It shows that the values and radial positions of $(u_z/u_x)_{max}$ at each phase were different, that is, the position of PVC at each phase was different. By comparing Figs. 11 (a) and 12, it shows that the velocity at F_1 became larger when the PVC approaches F_1. Another interesting phenomenon is that the PVC rotated around axisymmetric line at non-uniform angular velocity. The positions of $(u_z/u_x)_{max}$ at phase 0°, 144° and 216° are marked in Fig. 12 as T_1, T_2 and T_3 respectively. Seen from Fig. 12, the total radial displacement of PVC was 0.14 at process $T_1 \to T_2 \to T_3$, while the displacement was 0.03 at process $T_3 \to T_1$. The mean radial displacement rates $\Delta S/\Delta T$ of PVC at different process are list in Table 3. The variable ΔS represents normalized total radial displacement, ΔT represents the normalized time spent at each process, φ is the phase angle. The subscript "i" and "j" represent T_1, T_2 or T_3.

$$\Delta S = \mathrm{sum}(\Delta_{i,j}(r/R_p)) \tag{5}$$

$$\Delta\left(\frac{r}{R_p}\right)_{i,j} = \left.\frac{r}{R_p}\right|_j - \left.\frac{r}{R_p}\right|_i \tag{6}$$

$$\Delta T = \mathrm{sum}(\Delta T_{i,j}) \tag{7}$$

$$\Delta T_{i,j} = \frac{\varphi_j - \varphi_i}{360^\circ} \tag{8}$$

Seen from Table 3, the mean radial displacement rate at process $T_1 \to T_2 \to T_3$ was 0.217, while the rate at process $T_3 \to T_1$ was 0.075. It indicates that the PVC would rotate around axisymmetric line intermittently. This intermittency would be caused by the asymmetric radial vessel of pilot inlet. However, the intermittent motion did not affect the sinusoidal flow feature at F_1 position. The intermittency phenomenon was also observed by Dawson et al.[26,27]

The hotwire test results obtained under non-reacting flow condition are valuable. A large number of tests under reacting flow conditions with different combustor inlet temperature, inlet pressure, fuel–air-ratio and fuel-stage-ratio have been conducted for TeLESS combustor.[28,29] The PVC mode appeared in some reacting flow cases, while disappeared in other reacting flow cases. This phenomenon was similar to Syred's work.[14] Fig. 13 shows the dynamic pressure spectrum

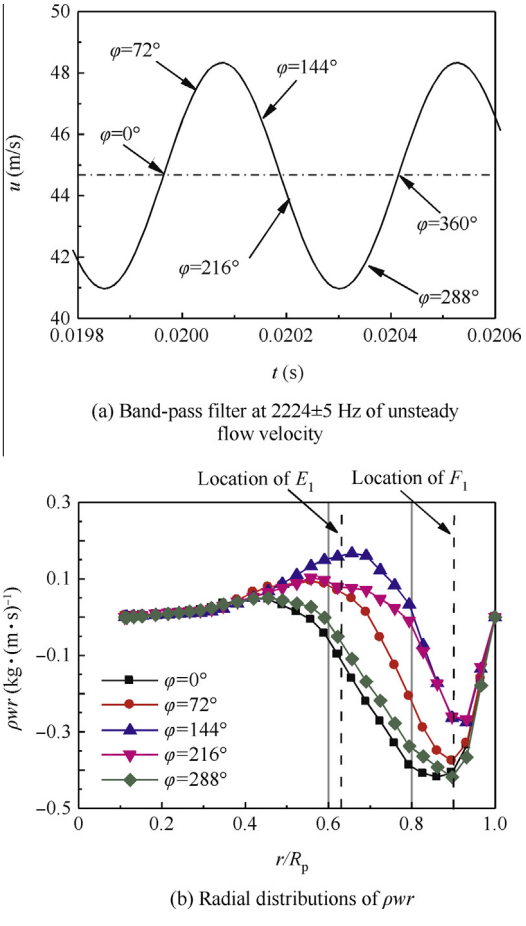

Fig. 11 Radial distributions of ρwr at different phases at the position of $x = 2$ mm (LES result).

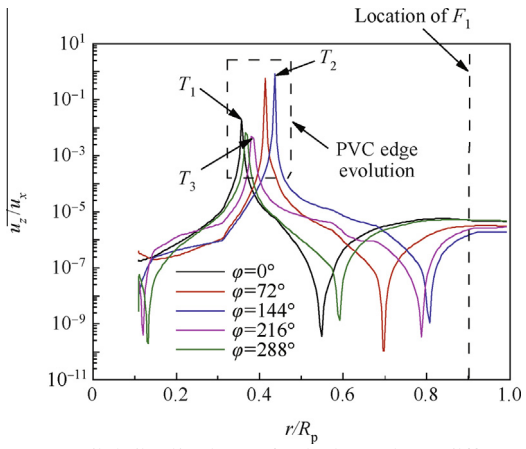

Fig. 12 Radial distributions of velocity ratio at different phases (LES result).

Table 3 Mean radial movement of PVC at $x = 2$ mm.

Process	Normalized time spent at each process ΔT	Normalized total radial displacement ΔS	Mean radial displacement rate $\Delta S/\Delta T$
$T_1 \rightarrow T_2 \rightarrow T_3$	0.6	0.13	0.217
$T_3 \rightarrow T_1$	0.4	0.03	0.075

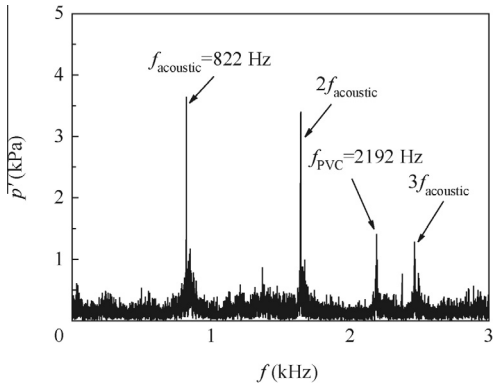

Fig. 13 Dynamic pressure spectrum under reacting flow condition for TeLESS combustor. (Inlet temperature is 750 K, inlet pressure is 1.1 MPa, air mass flow rate is 0.95 kg/s, fuel–air-ratio is 0.023, fuel-stage-ratio is 43%).

obtained from one of the reacting flow tests, the ordinate p' represents pressure oscillation component. The specturm can be distinguished by two kinds of movements. The one is combustor acoustic resonant(822 Hz) and its harmonic resonant, and the other one is PVC motion(2192 Hz).The detailed information about reacting flow test for TeLESS can be found in reference.[28]

5. Summary

Unsteady flow feature and its mechanism in TeLESS stratified swirl flow were investigated by combining hotwire measurement and large eddy simulation and several conclusions are listed as follows:

(1) Unsteady flow modes of 1126 Hz and 2244 Hz at pilot outlet were found in the hotwire test and unsteady flow was dominated by 2244 Hz mode. The velocity fluctuation intensity decayed convectively. And the maximum intensity occurred near pilot outlet shear layer.
(2) Mechanism of unsteady flow mode was investigated through LES method. The mesh dimension and time resolution were set based on the hotwire test results. The mode frequency prediction deviated from test by less than 1.4%. Although the mode amplitude prediction deviated largely from test, the predicted spatial distribution of fluctuated amplitude was similar to test results.
(3) The spiral structure of isobaric surface (99500 Pa) indicates that there was precessing vortex core in the pilot stage passage. Unsteady velocity spectra at several special positions were discussed. The periodic flow at the pilot outlet would be caused by the precessing motion. And the shear between 1st and 2nd counter swirl flow in pilot had a distinct damping effect on precessing motion.
(4) Different flow features existed along radial direction. The negative gradient $d(\rho wr)/dr$ indicated that the swirl flow was unstable.
(5) The variation of velocity ratio distribution at different phases indicates that the PVC rotated intermittently.
(6) The PVC motion frequency under non-reacting flow condition is slightly different from the frequency under reacting flow condition. Consequently, the investigation conducted under the non-reacting flow condition is meaningful and economical.
(7) The PVC motion would be a potential mechanism affecting the unsteady heat release, which depends on the fuel supply condition. To eliminate PVC's negative effects, it requires reducing the swirl number of pilot's 1st stage to decrease the PVC intensity as suggested in reference.[14]

Acknowledgement

Thanks for AVIC Commercial Aircraft Engine Co., Ltd.'s support on combustion instability investigation.

References

1. Smith R. Advanced low emissions subsonic combustor study. Washington, D.C.: NASA; 1998. Report No.: CR-1998-207931.
2. Kuentzmann P. Report of the independent experts to CAEP/8 on the second NO_X review & long term technology goals. Montreal, Canada: ICAO; 2010. Report No.: Doc-9953.
3. Lieuwen TC, Yang V. *Combustion instabilities in gas turbine engines*. Reston: AIAA; 2005.
4. Huang Y, Yang V. Dynamics and stability of lean-premixed swirl-stabilized combustion. *Prog Energy Combust Sci* 2009;**35**(4):293–364.
5. Fu ZB, Li JB, Lin YZ. Experimental investigation on ignition performance of LESS combustor. *Proceedings of the ASME turbo expo*. Vancouver, Canada. New York: ASME; 2011.
6. Lee HJ, Kim KT, Lee JG, Quay BD, Santavicca DA. An experimental study of the coupling of combustion instability mechanisms in a lean premixed gas turbine combustor. *Proceedings of the ASME turbo expo*. Orlando, USA. New York: ASME; 2009.
7. Lieuwen T, Neumeier Y, Zinn BT. The role of unmixedness and chemical kinetics in driving combustion instabilities in lean premixed combustor. *Combust Sci Technol* 1998;**135**(1–6):193–211.
8. Lee JG, Kim K, Santavicca DA. Measurement of equivalence ratio and its effect on heat release during unstable combustion. *Proc Combust Inst* 2000;**28**(1):415–21.
9. Nguyen QV. Measurements of equivalence ratio fluctuations in a lean premixed prevaporized (LPP) combustor and its correlation

to combustion instability. *Proceedings of the ASME turbo expo*. Amsterdam, Netherlands. New York: ASME; 2002.
10. Huang Y, Yang V. Bifurcation of flame structure in a lean-premixed swirl stabilized combustor: Transition from stable to unstable flame. *Combust Flame* 2004;**136**(3):383–9.
11. Sengissen AX, Giauque AV, Staffelbach GS, Porta M, Krebs W, Kaufmann P, et al. Large eddy simulation of piloting effects on turbulent swirling flames. *Proc Combust Inst* 2007;**31**(2):1729–36.
12. Bellow BD, Bobba MK, Seitzman JM, Lieuwen T. Nonlinear flame transfer function characteristics in a swirl-stabilized combustor. *J Eng Gas Turbines Power* 2007;**129**(4):954–61.
13. Balachandran R, Ayoola BO, Kaminski CF, Dowling AP, Mastorakos E. Experimental investigation of the nonlinear response of turbulent premixed flames to imposed inlet velocity oscillations. *Combust Flame* 2005;**143**(1):37–55.
14. Syred N. A review of oscillation mechanisms and the role of the precessing vortex core (PVC) in swirl combustion systems. *Prog Energy Combust Sci* 2006;**32**(2):93–161.
15. Steinberg AM, Arndt CM, Meier W. Parametric study of vortex structures and their dynamics in swirl-stabilized combustion. *Proc Combust Inst* 2013;**34**(2):3117–25.
16. Palies P, Durox D, Schuller T, Candel S. The combined dynamics of swirlers and turbulent premixed swirling flames. *Combust Flame* 2010;**157**(9):1698–717.
17. Qin H, Ding ZL, Li HT, Lin YZ, LI JB. Unsteady swirling flow in low emissions stirred swirls (LESS) combustor. *J Aerosp Power* 2015;**30**(7):1566–75 [Chinese].
18. Zhang M, Fu ZB, Lin YZ, Li JB. CFD study of NO_X emissions in a model commercial aircraft engine combustor. *Chin J Aeronaut* 2012;**25**(6):854–63.
19. Qin H, Ding ZL, Lin YZ, Li JB. Dynamic response characteristic of concentric stage swirling structure. *J Aerosp Power* 2015;**30**(4):793–9 [Chinese].
20. Hirshi G, Hiroyuki N, Takaya M, Shigeru T. Dynamic properties of combustion instability in a lean premixed gas-turbine combustor. *Chaos* 2011;**21**(1):013124–13134.
21. Wang S, Yang V, Hsiao G, Hsieh SY, Mongia HC. Large eddy simulation of gas turbine swirl injector flow dynamics. *J Fluid Mech* 2007;**583**:99–122.
22. Roux S, Lartigue G, Poinsot T, Meier U, Berat C. Studies of mean and unsteady flow in a swirled combustor using experiments, acoustic analysis and large eddy simulations. *Combust Flame* 2005;**141**(1):40–54.
23. Rayleigh L. On the stability of stratified flow. *Proc R Soc London* 1916;**93**:148–58.
24. Beer JM, Chigier NA, Davies TW, Bassindale K. Laminarization of turbulent flames in rotating environments. *Combust Flame* 1971;**16**:39–45.
25. Syred N, O'Doherty T, Froud D. The interaction of the precessing vortex core and reverse flow zone in the exhaust of a swirl burner. *J Power Energy* 1994;**208**(1):27–36.
26. Dawson JR, Rodrigues-Martinez VM, Syred N, O'Doherty T. The effect of expansion plane geometry on fluid dynamics under combustion instability in a swirl combustor. *Proceedings of 41st AIAA aerospace sciences meeting and exhibit*. Reno, Nevada. Reston: AIAA; 2003.
27. Dawson JR, Rodrigues-Martinez VM, Syred N, O'Doherty T. The effect of combustion instability on the structure of recirculation zones in confined swirling flames. *Combust Sci Technol* 2005;**177**(12):2349–71.
28. Qin H, Tang GQ, Lin YZ, Li JB. Influence of fuel stage ratio on pressure oscillation frequency of LESS combustor. *J Aerosp Power* 2015;**30**(6):1337–43 [Chinese].
29. Qin H, Fu ZB, Lin YZ, Li JB. Investigation on liner structure optimization based on pressure oscillation in combustors. *J Aerosp Power* 2015;**30**(5):1076–83 [Chinese].

Qin Hao is a Ph.D. candidate at School of Energy and Power Engineering, Beihang University. His area of research includes unsteady swirling flow, flame dynamics and combustion instability.

Lin Yuzhen is a professor and Ph.D. supervisor at School of Energy and Power Engineering, Beihang University. His main research interests are low emission combustion, combustion instability and supersonic combustion.

Li Jibao is the vice president and the chief engineer of AVIC Commercial Aircraft Engine Co., ltd. He is the project leader of civil aeroengine.